Scientific Reports

https://doi.org/10.1038/s41598-026-40165-7

Article in Press

# Valorization of *Sargassum wightii* through biochar production: development, characterization, and potential applications

Received: 14 October 2025

Accepted: 10 February 2026

Published online: 11 April 2026

Cite this article as: Raj R., S.S G., Sharaf S. *et al.* Valorization of *Sargassum wightii* through biochar production: development, characterization, and potential applications. *Sci Rep* (2026). https://doi.org/10.1038/s41598-026-40165-7

**Rehana Raj, Greeshma S.S, Sifana Sharaf, Niladri Shekhar Chatterjii, Arputharaj A, Laly S.J & Asha K.K**

# Valorization of *Sargassum wightii* through biochar production: Development, characterization, and potential applications

Rehana Raj[a], Greeshma S.S[b]., Sifana Sharaf[b], Niladri Shekhar Chatterjii[b], A Arputharaj[c], Laly S.J[b]., Asha K.K[a]

[a] Mumbai Research Centre; ICAR-Central Institute of Fisheries Technology, Vashi, Navi Mumbai, India, 400703

[b] ICAR-Central Institute of Fisheries Technology, Matsyapuri, Cochin, Kerala, India, 682029

[c] ICAR-Central Institute of Research on Cotton Technology, Matunga, Maharashtra, India, 400019

*Corresponding author:rajrehana9@gmail.com

Phone: + 022-278226017

**Abstract**

The valorization of marine biomass into functional materials offers a sustainable strategy for water purification within a circular bioeconomy framework. In this study, *Sargassum wightii* biomass was converted into biochar through controlled pyrolysis at 350, 500, and 600 °C, and the resulting materials were evaluated for water treatment applications. Increasing pyrolysis temperature resulted in reduced biochar yield but enhanced alkalinity and surface reactivity, driven by progressive carbonization and mineral enrichment. The biochars produced at higher temperatures exhibited favorable surface characteristics, including increased negative surface charge and mineral-associated active sites, which are advantageous for contaminant removal. The practical applicability of the biochars was demonstrated through adsorption studies using the pyrethroid pesticides cypermethrin and deltamethrin in spiked water systems. All biochars showed very high removal efficiencies, with biochar produced at 500 °C achieving the lowest residual pesticide concentrations, followed closely by biochar produced at 600 °C, while biochar produced at 350 °C showed comparatively lower performance. The enhanced adsorption at higher pyrolysis temperatures is attributed to improved pore development and aromatic carbon structures that promote strong hydrophobic and π–π interactions with pesticide molecules. Overall, *S. wightii*–derived biochar, particularly when produced at approximately 500 °C, demonstrates strong potential as a low-cost and sustainable adsorbent for pesticide-contaminated water treatment.

**Keywords**

Seaweed biochar, Pyrolysis temperature, *Sargassum wightii*, Surface characterization, Water purification, Sustainable biomass valorization

## Introduction

Ensuring the availability of clean water and maintaining sustainable food production systems remain pressing global challenges, as emphasized under the United Nations Sustainable Development Goals (SDGs) 6 and 2, which target universal access to safe water, sanitation, and food security by 2030. Rapid deterioration of freshwater quality caused by industrial effluents, agricultural runoff, synthetic dyes, and heavy metal contamination poses serious environmental and public health concerns, highlighting the need for efficient, low-cost, and environmentally sustainable remediation technologies [1]. Among emerging solutions, biochar has gained considerable attention for water treatment applications due to its tunable physicochemical properties and potential for sustainable production from renewable biomass. When derived from marine biomass, biochar further offers the added advantage of valorizing underutilized resources while supporting circular bioeconomy principles.

Biochar is produced via pyrolysis of organic biomass under oxygen-limited conditions, yielding a carbon-rich material with distinct surface chemistry, porosity, and mineral composition. These properties enable biochar to interact with a wide range of waterborne contaminants, including heavy metals, synthetic dyes, pesticides, pharmaceutical residues, and excess nutrients, through mechanisms such as electrostatic attraction, ion exchange, surface complexation, and pore filling [2,3]. Importantly, the adsorption performance of biochar is strongly influenced by pyrolysis temperature, which governs the evolution of surface functional groups, aromaticity, ash content, mineral phases, and surface charge characteristics [4]. Despite this understanding, the relationship between temperature-driven physicochemical changes and adsorption-relevant properties remains insufficiently resolved for many marine biomass–derived biochars.

Marine macroalgae have emerged as promising biochar feedstocks owing to their rapid growth rates, widespread availability, and intrinsically high mineral content, particularly alkali and alkaline-earth metals such as potassium, sodium, calcium, and magnesium [6]. Unlike lignocellulosic biomass, seaweeds contain lower lignin content and higher proportions of polysaccharides, leading to the formation of mineral-rich, high-ash biochars with distinctive surface reactivity and alkalinity [7]. Several studies have demonstrated the effectiveness of seaweed-derived biochar for water treatment. For example, Sargassum-based biochars have shown strong adsorption affinity toward cationic dyes and heavy metals, driven by mineral-mediated interactions and electrostatic attraction [8,9].

Among marine macroalgae, *Sargassum* species are of particular interest due to their recurrent seasonal blooms and associated disposal challenges in coastal regions. Previous studies have reported that *Sargassum*-derived biochars exhibit high alkalinity, thermal stability, and reactive mineral phases, supporting applications in dye adsorption, nutrient removal, and catalytic processes [10]. Additionally, seaweed-based biochar has been explored as a soil amendment, improving soil water retention, nutrient availability, and crop productivity, thereby contributing to SDG 2 objectives related to food security [11]. However, existing studies often focus on single pyrolysis conditions or activated biochars, with limited systematic evaluation of how controlled pyrolysis temperature influences adsorption-relevant properties such as surface charge, mineral phase distribution, functional group chemistry, and microstructural features.

Therefore, a clear knowledge gap exists regarding the temperature-dependent evolution of physicochemical characteristics of *Sargassum wightii*–derived biochar and how these characteristics relate to its suitability for adsorption-based water purification. In particular, the

combined influence of pyrolysis temperature on mineral enrichment, surface reactivity, and charge behavior—key determinants for the removal of cationic contaminants such as pesticides and metal ions—has not been comprehensively addressed.

In this context, the present study investigates the controlled pyrolysis of *Sargassum wightii* biomass at 350 °C, 500 °C, and 600 °C to elucidate the influence of thermal treatment on biochar yield, surface chemistry, mineral composition, and structural properties. Comprehensive characterization using FTIR, SEM, BET, ICP-OES, XRD, and zeta potential analyses is coupled with adsorption studies using pesticide-spiked water to establish the relevance of physicochemical properties to practical water treatment performance. The study aims to identify optimal pyrolysis conditions for producing mineral-rich seaweed biochar suitable for sustainable and environmentally relevant water purification applications.

**Results and Discussion**

This study systematically evaluated the influence of pyrolysis temperature on the production yield and alkalinity of biochar derived from *Sargassum wightii*, with the objective of tailoring its properties for potential application in water filtration systems. Pyrolysis temperature plays a decisive role in determining biochar quality, as it directly affects pore development, ash accumulation, surface functional chemistry, and overall adsorption behavior.

A clear inverse relationship was observed between pyrolysis temperature and biochar yield (Table 1). The yield declined from 49.1% at 350 °C to 42.8% at 500 °C, further decreasing to 39.6% at 600 °C. This progressive reduction can be attributed to intensified devolatilization and thermal decomposition of labile organic constituents at elevated temperatures, leading to increased mass

loss while promoting greater carbon stabilization and structural integrity [12]. Comparable temperature-dependent yield reductions have been consistently reported for both lignocellulosic and algal biomass feedstocks.

In contrast, the pH of the biochar exhibited a pronounced increase with rising pyrolysis temperature, reaching 10.64 at 350 °C and increasing to 11.41 at 500 °C, before stabilizing at approximately 11.40 at 600 °C (Table 1). The observed enhancement in alkalinity is primarily associated with the thermal degradation of acidic surface functional groups and the concomitant enrichment of inorganic ash components, particularly alkali and alkaline earth metal carbonates and oxides such as potassium, calcium, and magnesium [13]. This behavior is especially characteristic of seaweed-derived biochars, which inherently possess high mineral content, making them prone to elevated alkalinity following thermal conversion [14], & [15].

The stabilization of biochar pH observed between 500 and 600 °C indicates that the majority of acidic surface functionalities are thermally decomposed at temperatures close to 500 °C, beyond which additional heating predominantly promotes aromatic carbon condensation and structural ordering rather than further increases in alkalinity [16]. Comparable trends, characterized by declining biochar yield accompanied by elevated pH, have been consistently documented for *Sargassum* species and other macroalgal feedstocks [17].

From an application-oriented standpoint, a pyrolysis temperature of 500 °C represents an optimal compromise, providing a relatively high biochar yield while achieving pronounced alkalinity (pH-11.41). Although pyrolysis at temperatures exceeding 500 °C can enhance carbon stability and resistance to degradation, the associated reduction in material yield may adversely affect process efficiency and economic viability when scaled for practical implementation [18].

**FTIR Analysis**

The FTIR spectra of *Sargassum wightii* biochars produced at 350 °C (M-25453), 500 °C (M-25454), and 600 °C (M-25455) clearly demonstrate the progressive transformation of functional groups with increasing pyrolysis temperature (Figure 1). These changes reflect the transition from an oxygen-rich biopolymer matrix to a more aromatic and structurally condensed carbon material, consistent with typical biochar formation pathways [13], [19]–[22].

At 350 °C, the spectrum shows a broad O–H stretching band (3400–3200 $cm^{-1}$) (Figure 1) indicating abundant hydroxyl, hydrogen-bonded groups, and polysaccharide remnants from alginate and fucoidan [12]. Strong aliphatic C–H stretching bands at 2920 and 2850 $cm^{-1}$ reflect the presence of lipid and protein residues. The distinct carbonyl peak around 1740 $cm^{-1}$ indicates thermally labile carboxylic acids and ester functionalities, while C–O–C vibrations in the 1100–1000 $cm^{-1}$ region confirm the presence of carbohydrate structures [13]. These features indicate that 350 °C biochar retains high polarity, reactivity, and cation-exchange potential.

At 500 °C, substantial structural reorganization occurs (Figure 1). The weakening of the O–H band signifies dehydration and loss of bonded water. The disappearance of the 1740 $cm^{-1}$ carbonyl peak confirms decarboxylation and cleavage of ester linkages. Meanwhile, the strengthening of the band near 1620 $cm^{-1}$ indicates the formation of aromatic C=C and conjugated C=O systems, marking the onset of aromatic condensation [14]. The weakening of polysaccharide C–O bands (1100–1000 $cm^{-1}$) further reflects carbohydrate decomposition. These features represent a transitional stage—a balance between residual oxygenated groups and emerging aromaticity.

It was reported that wood-derived biochar produced at higher temperatures exhibits reduced oxygen-containing functionalities and increased aromaticity, as reflected by lower O/C and H/C ratios and enhanced structural order [23]. This supports the observed spectral changes in *Sargassum* biochar at 500 °C.

At 600 °C, the FTIR spectrum becomes dominated by strong aromatic C=C peaks around 1600 $cm^{-1}$, indicating well-developed aromatic clusters and graphitic domains (Figure 1). Aliphatic C–H stretching bands disappear, confirming volatilization of lipids and proteinaceous residues. The disappearance of carbohydrate-related peaks in the fingerprint region signifies near-total decomposition of polysaccharides and oxygenated biopolymers. These features align with the formation of a thermally stable, carbon-rich, hydrophobic structure characteristic of high-temperature biochars [13], [22].

Similar observations were made on the same temperature trend: biochars produced at higher temperatures (Biochar 700 °C) showed greater aromatic condensation, higher conductivity, stronger structural definition, and enhanced sorptive performance, supporting the structural interpretation for *Sargassum* biochar at 600 °C [23].

The FTIR findings are consistent with previous algal and lignocellulosic biochar studies showing that increasing pyrolysis temperature accelerates devolatilization, dehydration, and aromatization, leading to reduced polarity and enhanced structural stability [13], [21]. The low-temperature biochar (350 °C) is rich in functional groups suited for ion exchange and adsorption of polar contaminants. The 500 °C biochar presents mixed functionality, potentially advantageous for broad-spectrum adsorption. The 600 °C biochar possesses a highly aromatic, hydrophobic, and

stable matrix that is more suitable for long-term carbon storage, heavy-metal adsorption via π-complexation, and structural or electrochemical applications.

Further the earlier studies reported that functional interpretations by demonstrating that high-temperature biochars (700 °C) possess superior electrochemical activity, higher surface area, stronger adsorption-driven accumulation, and better interaction with analytes, due to the increased aromaticity, porosity, and structural integrity of the carbon matrix [23]

Collectively, the FTIR analysis confirms that pyrolysis temperature is the key factor shaping the chemical structure and functional performance of *Sargassum wightii* biochar. The progressive loss of oxygenated groups and development of aromatic networks with temperature parallels both earlier findings of the [23]. These structural transitions explain the improved stability, conductivity, and application potential of high-temperature biochars while highlighting the reactivity advantage of low-temperature materials.

**Brunauer–Emmett–Teller (BET) analysis**

Brunauer–Emmett–Teller (BET) analysis of *Sargassum wightii*–derived biochars produced at 350, 500, and 600 °C showed a clear temperature-dependent evolution in surface area and porosity. The BET surface areas were 5.994 $m^2/g$ (350 °C), 5.277 $m^2/g$ (500 °C), and 8.959 $m^2/g$ (600 °C). Overall, surface area exhibited a non-linear trend with increasing pyrolysis temperature, characterized by a slight decrease at the intermediate temperature followed by a pronounced increase at the highest temperature.

Biochar produced at 350 °C exhibited a moderate surface area, indicating limited pore accessibility at lower thermal severity. A marginal reduction in surface area was observed for biochar produced

at 500 °C, suggesting restricted pore development under intermediate pyrolysis conditions. In contrast, biochar produced at 600 °C showed a marked increase in surface area, reflecting enhanced pore opening and improved micro- and mesoporous structure at higher pyrolysis temperature.

The observed non-linear trend in BET surface area reflects temperature-driven structural transformations during pyrolysis. At lower temperatures, incomplete devolatilization and the presence of residual organic matter can limit pore accessibility, while intermediate temperatures may lead to temporary pore obstruction due to tar deposition and partial restructuring of the carbon matrix, a behavior commonly reported for lignocellulosic biochars during mid-range pyrolysis [16]. Similar suppression of surface development at intermediate temperatures has also been reported for wood-derived biochars.

At higher pyrolysis temperature (600 °C), the substantial increase in surface area indicates extensive volatilization of organic components, aromatization of the carbon framework, and opening of previously sealed pore structures, leading to enhanced micro- and mesopore formation. Comparable increases in surface area and pore volume with increasing pyrolysis temperature have been reported when temperatures are raised from 400 to 700 °C, attributed to decomposition, condensation, and restructuring of the carbon matrix [23].

Seaweed-derived biochars are generally characterized by lower surface areas (typically 4–10 $m^2/g$ across 350–650 °C) compared to lignocellulosic biochars, largely due to their high ash and mineral content (Ca, K, Na, and Mg), which can restrict pore expansion and compete with carbon for structural rearrangement [17]. Nevertheless, the trend observed in the present study—an initial decline followed by a significant increase in surface area at ≥600 °C—parallels findings reported

for agricultural-residue biochars, where extensive devolatilization and carbon reorganization at higher temperatures (>600 °C) markedly enhance porosity [6].

Increasing pyrolysis temperature also promotes the formation of alkaline mineral oxides and the removal of acidic oxygen-containing functional groups, contributing to higher pH and improved surface activation [18]. Previous studies on wood-derived biochar further confirm that higher pyrolysis temperatures enhance aromatic condensation, reduce oxygen content, and improve pore connectivity, thereby increasing adsorption potential for contaminant removal applications [23].

Although the BET surface areas of *Sargassum wightii* biochars remain modest relative to activated carbons, the combined effects of pore development, reactive surface functionality, and mineral-rich composition enhance their suitability for environmental remediation. In particular, the increased surface area observed at 600 °C suggests that high-temperature pyrolysis is advantageous for improving adsorption potential toward dyes, metals, pesticides, and other waterborne pollutants. The synergistic role of mineral phases, as highlighted by [19], may further enhance adsorption through electrostatic interactions, surface complexation, and catalytic effects, which are critical for water purification processes.



**Mineral analysis of the biochar**

ICP–OES analysis (Tables 2–4) showed that alkali and alkaline-earth metals (K, Na, Ca, and Mg) were the dominant inorganic constituents in *Sargassum wightii* biochars produced at all three pyrolysis temperatures (350, 500, and 600 °C). Across the temperature range, a clear enrichment of these major cations was observed with increasing pyrolysis temperature.

Biochar produced at 350 °C (S1) exhibited high concentrations of K, Na, Ca, and Mg, reflecting the intrinsically mineral-rich nature of macroalgal biomass. With increasing pyrolysis temperature

to 500 °C (S2), the overall mineral composition remained similar, while biochar produced at 600 °C (S3) showed a pronounced increase in alkali and alkaline-earth metal concentrations, indicating temperature-dependent mineral concentration.

Trace metals displayed distinct temperature-related trends. Cadmium concentrations decreased progressively with increasing pyrolysis temperature, whereas arsenic concentrations increased from S1 to S3. Other ash-forming elements, including Ti, B, Ba, Sr, and Fe, also showed moderate enrichment at higher temperatures.

The observed enrichment of alkali and alkaline-earth metals with increasing pyrolysis temperature reflects the progressive loss of volatile organic matter and enhanced carbonization, which concentrate inorganic constituents within the biochar matrix [28–30]. Similar mineral concentration effects driven by dehydration, decarboxylation, and solid-phase rearrangement have been widely reported during thermochemical processing of biomass, including hydrothermal carbonization studies.



Macroalgae are known to accumulate high levels of K, Na, Ca, and Mg, and consequently, even moderate-temperature pyrolysis yields mineral-dense, high-ash biochars. The present results align well with previous studies on seaweed-derived biochars, which emphasize consistently elevated mineral contents and their relevance to alkalinity, ion-exchange capacity, and surface complexation behavior [31,32]. The enhanced retention of K and Na at 600 °C suggests strong preservation of alkali and alkaline-earth metal species, which are known to catalyze thermal transformations and contribute to surface reactivity.

High concentrations of Ca and Mg are particularly relevant for applications involving phosphate precipitation, hardness-ion binding, and alkaline buffering, supporting the potential utility of these biochars in water treatment systems [33,34]. Comparable mineral retention and enrichment at elevated temperatures have also been documented in hydrothermal carbonization studies, where increasing thermal severity yields carbon-dense, mineral-rich solids.

The decline in Cd concentration with increasing temperature is consistent with temperature-sensitive transformations of trace metals, including partial volatilization or stronger immobilization within condensed mineral matrices, as reported previously [35]. In contrast, the increase in As concentration with temperature is most likely attributable to mass-loss-driven concentration effects during pyrolysis. This trend underscores the importance of assessing trace-metal leachability prior to environmental application, in agreement with reviews highlighting mineral composition as a determinant of both adsorption functionality and environmental risk [36].

Other ash-forming elements (Ti, B, Ba, Sr, and Fe) exhibited moderate temperature-related enrichment, a behavior typical of macroalgal biochars and distinct from lignocellulosic biochars due to differences in intrinsic mineral composition and oxide stability [37]. These trends are consistent with thermochemical behavior reported in earlier studies, where increasing temperature promotes dehydration, decarboxylation, and structural condensation, resulting in a more stable and mineral-rich carbon matrix [38].

Overall, increasing pyrolysis temperature from 350 to 600 °C resulted in progressive concentration of major cations and trace minerals in *Sargassum wightii* biochar. Functionally, biochar produced at lower temperature retained abundant minerals with more labile organic fractions, intermediate temperature biochar represented a transitional stage of carbonization, and high-temperature

biochar exhibited the greatest mineral enrichment and structural stability. Such mineral-rich biochars are well suited for applications involving alkaline buffering, cation exchange, and nutrient or hardness-ion uptake, although the elevated arsenic content at higher temperatures necessitates careful evaluation of leaching behavior prior to field deployment [34].

**Zeta Potential Analysis**

The zeta potential of biochar (Table 5) provides valuable information on its surface charge characteristics, colloidal stability, and electrostatic interactions with charged pollutants in aqueous environments. The present study examined the zeta potential of brown seaweed-derived biochar produced at three pyrolysis temperatures—350 °C (Sample A), 500 °C (Sample B), and 600 °C (Sample C)—under neutral pH conditions (pH 7). The measured zeta potential values were –3.03 mV, –1.28 mV, and –7.93 mV, respectively (Table 5).



At 350 °C, the biochar exhibited a moderately negative surface charge (–3.03 mV), which can be attributed to the retention of oxygenated functional groups such as hydroxyl (–OH), carboxyl (–COOH), and sulfate ester moieties originating from the seaweed matrix. These polar groups, partially preserved under mild pyrolysis, contribute to colloidal stability and facilitate electrostatic attraction toward cationic species such as $Pb^{2+}$, $Cd^{2+}$, and $Cu^{2+}$ ions, as well as positively charged organic dyes. Similar observations were reported by [19] who demonstrated that low-temperature biochars maintain labile surface functionalities enhancing their affinity for heavy metals and nutrients.

At 500 °C, the zeta potential value decreased to –1.28 mV, indicating a reduction in the net negative surface charge. This decline is primarily due to the progressive decomposition of

oxygenated functional groups and the transition of the carbon matrix toward a more aromatic and hydrophobic structure. The lower zeta potential suggests diminished colloidal stability and weaker electrostatic interactions with cations. However, increased structural order and porosity at this temperature can promote physical adsorption through pore filling and hydrophobic interactions. These results align with findings by [35] who noted that intermediate-temperature biochars exhibit enhanced porosity despite reduced surface polarity, enabling a balanced adsorption mechanism driven by both electrostatic and physical forces.

At 600 °C, the biochar exhibited a more pronounced negative zeta potential (–7.93 mV), suggesting a significant increase in surface charge compared to the lower-temperature samples. Extensive carbonization at this temperature leads to the formation of condensed aromatic domains while exposing mineral residues such as silicates and oxides of Ca, Mg, and Fe. The deprotonation of hydroxyl groups associated with these mineral phases contributes to the observed increase in negative charge. This enhanced electrostatic potential favors strong interactions with cationic contaminants, improving the suitability of high-temperature biochar for heavy metal and dye adsorption applications. Comparable trends have been reported by [37] and [39], highlighting that mineral–biochar interfaces play a dominant role in surface charge development at elevated pyrolysis temperatures.

Hence, the results demonstrate a temperature-dependent evolution of surface electrokinetic properties Sample A (350 °C) retained oxygen-rich functional groups and good colloidal stability, Sample B (500 °C) showed reduced surface charge but improved porosity, and Sample C (600 °C) exhibited enhanced negative zeta potential due to mineral-associated charge formation. These findings confirm that pyrolysis temperature critically governs the surface charge characteristics

and potential adsorption efficiency of seaweed-derived biochar, consistent with previous reports on algal and lignocellulosic feedstocks [39] & [40].

**Scanning Electron Microscopy**

The SEM micrographs (Fig. 2–4) revealed clear temperature-dependent changes in the morphology of seaweed-derived biochars. At 350 °C, the biochar exhibited rough, flaky surfaces with heterogeneous fragments ranging from nanoscale particles to larger plate-like structures, reflecting uneven matrix degradation and volatile release [41]. Such morphology is consistent with low-temperature macroalgal biochars known to offer abundant active sorption sites [42]. At 500 °C, the material showed more aggregated and porous structures with finer particle distribution, indicating enhanced fragmentation and exposure of functional sites, similar to earlier reports on intermediate-temperature seaweed biochars [43]. At 600 °C, pronounced plate-like and granulated morphologies were observed, reflecting partial preservation of fibrous residues alongside brittle fragmentation under higher thermal severity [44]. Overall, the SEM analysis confirms that increasing pyrolysis temperature promotes greater porosity, fragmentation, and structural heterogeneity, which collectively enhance the adsorptive potential of seaweed biochars for pollutants [45].

**X-ray Diffraction Analysis (XRD)**

XRD patterns of the three seaweed biochars were recorded under identical instrumental conditions (Rigaku MiniFlex 300/600; Cu radiation; 40 kV, 15 mA; 2θ range 3–80°; step width 0.02°; scan speed 6°/min; θ/2θ geometry with specimen rotation). The diffractograms are dominated by sharp reflections, indicating a high contribution of crystalline mineral ash phases—typical for

macroalgae/seaweed biochars due to their inherently high inorganic salt content (Figure 5, 6, 7). This behavior is widely reported for macroalgae-derived biochars, where alkali/alkaline-earth salts and carbonates contribute strong crystalline peaks compared with lignocellulosic biochars [46].

Across all three samples, the most intense peak occurs near 2θ ≈ 28.4–28.6° (S1: 28.582°; S2: 28.361°; S3: 28.437°), accompanied by strong reflections around 31.7–31.8° (S1: 31.817°; S2: 31.721°; S3: 31.7869°). This peak set is consistent with the presence of alkali halide ash phases—commonly assigned to sylvite (KCl) and halite (NaCl) in biomass/biochar XRD literature—reflecting the salt-rich nature of seaweeds. Similar identification of KCl-related reflections around ~28.4° in biochar/mineralized biomass systems has been reported by prior studies and compilations [47]. Notably, the higher-temperature biochars (S2 and S3) show a richer set of sharp, high-angle reflections (e.g., ~56–58°, ~66°, ~73–75°), indicating enhanced ash crystallinity and/or improved ordering of mineral phases with increasing pyrolysis temperature. This is expected because progressive devolatilization concentrates inorganic constituents in the char matrix, and elevated temperatures promote crystallization/sintering of mineral salts in the ash fraction—an effect highlighted in macroalgae-biochar studies that include XRD-based mineral identification [46].

All three samples show a clear reflection near 2θ ≈ 29.4–29.6° (S1: 29.573°; S2: 29.389°; S3: 29.440°) (Figure 5,6,7). In biochar systems, a peak in this region is frequently attributed to carbonate minerals, particularly calcite ($CaCO_3$), and carbonate persistence in chars is often linked to Ca- and Mg-rich ash chemistry. Reports on biochar XRD interpretation commonly discuss calcite-associated reflections (including d-spacings around ~3.03 Å / ~29.4° 2θ) as part of mineral ash assemblages [48]. With increasing pyrolysis temperature, carbonates can partially decompose

and/or react to form oxide phases (e.g., CaO, MgO) depending on residence time, heating rate, and local $CO_2$ partial pressure. In your dataset, S3 (600 °C) exhibits additional/stronger reflections in regions often associated with Ca-bearing oxides (e.g., ~37° and ~54°), which may indicate partial conversion of carbonate to oxide-type phases at higher temperature. This interpretation is consistent with the general thermal chemistry of ash in biochars and is frequently discussed in advanced biochar characterization work where XRD is used alongside complementary techniques to track mineral transformations [46].

Seaweed biochars often show comparatively weaker "carbon ordering" signatures in XRD because strong ash peaks dominate the pattern. Nevertheless, reflections around ~24–27° (e.g., S2: 26.614°; S3: 26.698°) can be discussed as overlapping contributions from turbostratic carbon (002) and/or mineral contributions (e.g., silicates/quartz in some biomass-derived chars). The earlier studies frequently emphasize that, compared to terrestrial biomass chars, algal/seaweed chars show XRD patterns where mineral reflections are prominent and carbon-related features are less diagnostic unless ash is removed or carbon ordering is probed by Raman/HT-XRD [46].



Overall, the key outcome from your three-temperature series is that increasing pyrolysis temperature (350 → 600 °C) strengthens and multiplies crystalline mineral ash reflections, consistent with (a) ash enrichment and crystallization of alkali halides and carbonates, and (b) possible onset of carbonate-to-oxide transformation at the highest temperature, while the carbon matrix remains largely masked by mineral crystallinity in the diffractograms.

**Application of Seaweed-Derived Biochar for the Removal of Pesticides from Water.**

The present study evaluates the adsorption efficiency of seaweed-derived biochar produced at different pyrolysis temperatures (350, 500, and 600 °C) for the removal of pyrethroid pesticides from water (Table 6). Cypermethrin and deltamethrin were selected as model hydrophobic pesticides, and their removal was assessed over a six-day contact period. Comparative analysis was performed to elucidate the influence of pyrolysis temperature on pesticide adsorption performance, in line with earlier reports highlighting the strong affinity of pyrethroids toward carbonaceous adsorbents with well-developed porosity and surface functionality [49].

The adsorption performance of seaweed-derived biochar pyrolysed at 350 °C was evaluated by comparing pesticide concentrations in spiked water on the 0th and 6th day. On the 0th day, cypermethrin and deltamethrin concentrations were 650.25 µg/L and 771.60 µg/L, respectively, indicating the initial spiking levels before significant adsorption occurred. After six days of contact with the biochar, a drastic reduction in pesticide residues was observed, with cypermethrin decreasing to 0.21 µg/L and deltamethrin to 0.19 µg/L, corresponding to removal efficiencies exceeding 99.9% for both pesticides. The pronounced decline over time highlights the strong adsorption affinity of 350 °C biochar toward hydrophobic pyrethroid pesticides, likely driven by surface functional groups and pore structure. Similar high deltamethrin removal efficiencies have been reported for activated biochar systems, where adsorption was primarily attributed to surface chemistry and accessible pores facilitating hydrophobic interactions [50].

The adsorption efficiency of seaweed biochar pyrolysed at 500 °C was assessed by comparing pesticide concentrations in spiked water on the 0th and 6th day. Initial cypermethrin and deltamethrin concentrations were 675.77 µg/L and 820.26 µg/L, respectively. After six days of

contact with the 500 °C biochar, pesticide residues were reduced to 0.081 µg/L for cypermethrin and 0.065 µg/L for deltamethrin, corresponding to removal efficiencies greater than 99.9%. The enhanced removal observed at 500 °C compared to lower pyrolysis temperatures can be attributed to increased surface area, improved pore development, and higher aromaticity of the biochar, which favor strong hydrophobic and π–π interactions with pyrethroid pesticides. These mechanisms are consistent with earlier findings on biochar pyrolysed at around 500 °C and activated carbon materials, where pore-filling and π–π electron donor–acceptor interactions were identified as dominant adsorption pathways for pyrethroid compounds such as lambda-cyhalothrin [51].

The adsorption performance of seaweed-derived biochar pyrolysed at 600 °C was also evaluated over the same contact period. On the 0th day, cypermethrin and deltamethrin concentrations were 463.72 µg/L and 731.09 µg/L, respectively, representing the initial pesticide load prior to adsorption. After six days of treatment with 600 °C biochar, pesticide residues were markedly reduced to 0.088 µg/L for cypermethrin and 0.050 µg/L for deltamethrin, again corresponding to removal efficiencies exceeding 99.9%. The high adsorption efficiency at 600 °C can be attributed to enhanced carbonization, increased aromaticity, and well-developed pore structures, which promote strong hydrophobic and π–π interactions with pyrethroid compounds. Comparable trends have been reported for high-surface-area KOH-activated carbons, where deltamethrin removal efficiencies were strongly correlated with aromatic carbon frameworks and mesoporous structures, as confirmed through kinetic and isotherm studies [51].

Therefore, seaweed-derived biochar exhibited exceptionally high adsorption efficiencies (>99.9%) for both cypermethrin and deltamethrin across all pyrolysis temperatures tested. Among them, biochar produced at 500 °C demonstrated the most effective removal, achieving the lowest residual

pesticide concentrations, followed closely by 600 °C biochar, while 350 °C biochar showed slightly higher residual levels. The superior performance at higher temperatures is attributed to enhanced surface area, pore development, and aromatic carbon structures that promote strong hydrophobic and π–π interactions, in agreement with previously reported adsorption mechanisms for pyrethroid pesticides using activated biochar and carbon-based adsorbents [49,50]. Collectively, these results confirm seaweed biochar—particularly when pyrolysed at ~500 °C—as a highly efficient, low-cost adsorbent for pesticide-contaminated water treatment.

**Conclusion**

The present investigation demonstrates that *Sargassum wightii* can be effectively valorized into biochar through controlled pyrolysis, offering a multifunctional material with significant potential for environmental remediation. The systematic evaluation across pyrolysis temperatures revealed a clear trade-off between yield, alkalinity, and structural stability. While low-temperature biochars retained abundant oxygenated functional groups conducive to cation exchange, higher temperatures promoted aromatic condensation, enhanced porosity, and enrichment of mineral phases. These transitions were reflected in the FTIR spectra, SEM morphologies, BET surface areas, and zeta potential measurements, collectively highlighting the decisive role of thermal severity in governing surface chemistry and adsorption behavior.

The substantial presence of alkali and alkaline-earth elements (K, Na, Ca, and Mg) further enhanced the functional attributes of seaweed biochar by enabling electrostatic interactions, catalytic activity, and buffering capacity in aqueous systems. Importantly, biochars prepared at ~500–600 °C provided an optimal balance of yield, alkalinity, porosity, and negative surface charge, making them particularly effective for contaminant removal. This was conclusively

demonstrated through application studies using cypermethrin- and deltamethrin-spiked water, where biochars achieved exceptionally high removal efficiencies (>99.9%) after six days of contact, with residual pesticide concentrations reduced to sub-µg/L levels. The superior adsorption performance observed at 500 °C and 600 °C is attributed to enhanced surface area, well-developed pore structures, and increased aromaticity, facilitating strong hydrophobic and π–π interactions with pyrethroid pesticides.

In conclusion, the integrated characterization and application results confirm that seaweed-derived biochar—especially when produced at ~500 °C—functions as a highly efficient, low-cost adsorbent for the removal of hydrophobic pesticide residues from contaminated water. Beyond water purification, the valorization of *S. wightii* into functional biochar supports circular bioeconomy principles by converting marine biomass into high-value environmental materials, thereby contributing directly to sustainable resource management and global clean water initiatives.



## Materials and Methods

### Raw Material Preparation

Brown seaweed (*Sargassum wightii*) was collected from the R.K. Algae Project Centre, Meenavar Colony, Mandapam, Ramanathapuram District, Tamil Nadu, India, primarily during the months of August to September. The collection was carried out during daytime under natural coastal environmental conditions, washed thoroughly with freshwater to remove adhering salts, sand, and epiphytes, and shade-dried until a constant weight was obtained. The dried biomass was crushed

into small fragments (2–5 mm) using a laboratory grinder and stored in airtight containers until further use.

**Biochar Production**

The dried and crushed biomass was pyrolyzed under oxygen-limited conditions in a programmable muffle furnace. Three different pyrolysis temperatures (350 °C, 500 °C, and 600 °C) were employed with a heating rate of 10 °C/min and a residence time of 2 h at the final temperature. After pyrolysis, the furnace was allowed to cool naturally to room temperature. The obtained biochar samples were collected, weighed, and stored in desiccators to avoid moisture uptake.

**Yield Determination**

The yield of biochar was calculated as the ratio of the dry weight of biochar produced to the dry weight of the original biomass, expressed as a percentage, using the equation:

$$Biochar\ yield\ (\%\ \text{dry weight basis}) = \frac{Wb}{W0} \times 100$$

where $W_b$ and  is the weight of the biochar obtained after pyrolysis (g), and $W_0$ is the initial dry weight of the raw biomass (g).

**Characterization of Biochar**

**pH**

Biochar slurry (1:20, w/v in distilled water) was prepared, and the pH of the resultant slurry was determined using a calibrated pH meter (EcoScan pH 5, EUTECH Instruments).

**Fourier Transform Infrared Spectroscopy (FTIR)**

Fourier Transform Infrared Spectroscopy (FTIR) was performed in the range of 4000–400 $cm^{-1}$ to identify functional groups present on the biochar surface. The analysis was performed using a Nicolet iS10 FT-IR spectrometer (Thermo Fisher Scientific India Pvt. Ltd., Mumbai) in the transmittance mode.

**Surface Area and Porosity**

Brunauer–Emmett–Teller (BET) surface area and pore volume were determined using $N_2$ adsorption–desorption isotherms at 77 K. BET analysis was performed on biochar samples produced at all three pyrolysis temperatures (350 °C, 500 °C, and 600 °C) to systematically evaluate the temperature-dependent evolution of crystalline phases and surface area characteristics



**Mineral analysis**

Determination of mineral content was performed following AOAC guidelines [52]. Biochar samples (≈1 g) were subjected to microwave-assisted acid digestion using concentrated nitric acid and hydrogen peroxide. The digested solutions were diluted with ultrapure water and analyzed using inductively coupled plasma–optical emission spectrometry (ICP-OES; Thermo Fisher Scientific).

Calibration was carried out using certified multi-element standard solutions, and five-point calibration curves were prepared for both major minerals and trace metals, yielding correlation coefficients ($R^2$) ≥ 0.999. Yttrium was used as an internal standard to ensure analytical accuracy.

All measurements were conducted under optimized instrumental conditions as recommended by the manufacturer.

**Zeta potential analysis**

The surface charge characteristics of the seaweed-derived biochar samples produced at three different pyrolysis temperatures (350 °C, 500 °C, and 600 °C) were evaluated through zeta potential analysis. Measurements were carried out using a NiComP 380 ZLS zeta potential analyzer. The surface charge characteristics of seaweed-derived biochar samples were determined using a Zeta Potential Analyzer. Approximately 3–4 mL of each biochar suspension was transferred into a clean cuvette and positioned in the instrument's sample holder for intensity verification. When the measured scattering intensity exceeded the optimal range, the sample was appropriately diluted using deionized (DI) water to achieve suitable concentration. Prior to zeta potential measurement, the hydrodynamic particle size of the dispersion was assessed to confirm that it was within the instrument's measurable range. Subsequently, the system was switched to the zeta potential mode, and measurements were recorded in triplicate to ensure data reproducibility.



**Scanning Electron Microscopy (SEM) analysis**

Scanning Electron Microscopy (SEM) (Model: SNE-Alpha, SEC Co., Ltd, SUWON, 16648, South Korea) was used to observe surface texture, pore development, and structural changes across pyrolysis temperatures.

**X-ray Diffraction Analysis (XRD)**

The crystalline structure and mineral phases of the seaweed-derived biochar produced at a pyrolysis temperature of 350 °C were analyzed using powder X-ray diffraction (XRD). The biochar sample was finely ground to obtain a homogeneous powder and analyzed in θ–2θ geometry using Cu Kα radiation (λ = 1.5406 Å). Diffraction patterns were recorded over a 2θ range of 5–65° with a step size of 0.02° under continuous scanning conditions. The powdered sample was uniformly mounted on a low-background sample holder to minimize preferred orientation effects. The obtained diffractograms were subjected to background correction and peak analysis, and crystalline phases were identified by comparing the diffraction peaks with standard reference patterns from the International Centre for Diffraction Data (ICDD) database. XRD analysis was used to assess the degree of crystallinity and mineralogical transformations occurring in the seaweed biochar as a result of pyrolysis. XRD was performed on biochar samples produced at all three pyrolysis temperatures (350 °C, 500 °C, and 600 °C) to systematically evaluate the temperature-dependent evolution of crystalline phases and surface area characteristics.



**Application of Seaweed-Derived Biochar for the Removal of Pesticides from Water**

Analytical-grade pesticide standards of cypermethrin and deltamethrin (PESTANAL®, Sigma-Aldrich, USA) were used for adsorption studies following established procedures [53] with minor modifications. Individual stock solutions (1000 ppm) of each pesticide were prepared using suitable analytical-grade solvents. Working solutions of 1 ppm were freshly prepared from the stock solutions and used to spike Milli-Q water (Milli-Q® SQ 2Series Water Purification Systems; Merck Millipore). The spiked solutions were continuously stirred to ensure uniform distribution of the pesticides.

Seaweed-derived biochar produced at three pyrolysis temperatures (350 °C, 500 °C, and 600 °C) was used as the adsorbent material. Biochar was added to the pesticide-spiked water samples at a concentration of 5% (w/v), and the suspensions were maintained under continuous agitation at room temperature to facilitate effective contact between the biochar and dissolved pesticides. All adsorption experiments were conducted in triplicate to ensure reproducibility.

Samples were collected at 0th day (initial concentration) and 6th day, which was considered sufficient to attain adsorption equilibrium based on previous studies reporting equilibrium uptake of hydrophobic pesticides by biochar within prolonged contact periods under aqueous conditions. The 6-day contact period was selected as sufficient to attain adsorption equilibrium, based on earlier studies on hydrophobic pesticide uptake by biochar under aqueous conditions [54] and the observation that further contact did not result in appreciable changes in residual pesticide concentration.

After the designated contact period, samples were filtered and analyzed for residual pesticide concentrations.



Residual concentrations of cypermethrin and deltamethrin were quantified in accordance with IS 3025 (Part 1) guidelines using gas chromatography–tandem mass spectrometry (GC–MS/MS). The method detection limit for both pesticides was 0.01 mg/kg.

**Acknowledgments**

The authors thank Director, Indian Council of Agriculture Research-Central Institute of Fisheries Technology, Cochin India for providing facilities to undertake this work.

- **Authors Contribution**

- Rehana Raj contributed to the conception and design of the study, analysis and interpretation of data and Manuscript drafting. Sifana Sharaf, Niladri Shekhar Chatterjii, A Arputharaj, & Laly S.J contributed in providing the resources and in carrying out analysis. Greesham S.S. and Asha K.K contributed in revising it critically for important intellectual content.

**Declaration**

- Authors declare that there is no conflict of Interest and all authors are aware of the submission of the manuscript
- **Funding**

This research did not receive any specific grant from funding agencies

**Declaration of generative AI in scientific writing**

Generative AI and AI-assisted technologies were used in the writing process to improve the readability and language of the manuscript

**Reference**

1. Zeghioud, H., Fryda, L., Djelal, H., Assadi, A., & Kane, A. (2022). A comprehensive review of biochar in removal of organic pollutants from wastewater: Characterization, toxicity, activation/functionalization and influencing treatment factors. *Journal of Water Process Engineering*, *47*, 102801.
2. Pech-Rodríguez, W. J., Meléndez-González, P. C., Hernández-López, J. M., Suarez-Velázquez, G. G., Sarabia-Castillo, C. R., & Calles-Arriaga, C. A. (2024).

Pharmaceutical Wastewater and Sludge Valorization: A Review on Innovative Strategies for Energy Recovery and Waste Treatment. *Energies*, *17*(20), 5043.

3. Inyang, M.I., Gao, B., Yao, Y., Xue, Y., Zimmerman, A., Mosa, A., Pullammanappallil, P., Ok, Y.S. and Cao, X., 2016. A review of biochar as a low-cost adsorbent for aqueous heavy metal removal. *Critical reviews in environmental science and technology*, *46*(4), pp.406-433.
4. Gul, S., Whalen, J. K., Thomas, B. W., Sachdeva, V., & Deng, H. (2015). Physico-chemical properties and microbial responses in biochar-amended soils: mechanisms and future directions. *Agriculture, ecosystems & environment*, *206*, 46-59.
5. Huang, Q., Song, S., Chen, Z., Hu, B., Chen, J., & Wang, X. (2019). Biochar-based materials and their applications in removal of organic contaminants from wastewater: state-of-the-art review. *Biochar*, *1*(1), 45-73.
6. Martínez-Meraz, C., González-Fernández, L. A., Medellín-Castillo, N. A., López-Cruz, C. M., Reyes-Hernández, J., Castillo-Ramos, V., & Sánchez-Polo, M. (2023). Sargassum biomass-derived biochars for ibuprofen removal from water: Adsorption and kinetics. *MRS Advances*, *8*(23), 1377-1384.
7. Manohara, H. M., Nayak, S. S., Franklin, G., Nataraj, S. K., & Mondal, D. (2021). Progress in marine derived renewable functional materials and biochar for sustainable water purification. *Green Chemistry*, *23*(21), 8305-8331.
8. Jafarian, S., Bolouk, A. M. L., Norouzian, R. S., Taghavi, S., Mousavi, F., Kianpour, E., & Signoretto, M. (2023). Sargassum macro-algae-derived activated bio-char as a sustainable and cost-effective adsorbent for cationic dyes: A joint experimental and DFT study. *Colloids and Surfaces A: Physicochemical and Engineering Aspects*, *678*, 132397.

**9.** Mohammed, A., Mohammed, C., Mautner, A., Kistow, M., Chaitram, P., Bismarck, A., & Ward, K. (2024). On the performance of Sargassum-derived calcium alginate ion exchange resins for Pb2+ adsorption: batch and packed bed applications. *Environmental Science and Pollution Research*, *31*(21), 31224-31239.

**10.** Hung, C. M., Huang, C. P., Cheng, J. W., Chen, C. W., & Dong, C. D. (2021). Production and characterization of a high value-added seaweed-derived biochar: Optimization of pyrolysis conditions and evaluation for sediment treatment. *Journal of Analytical and Applied Pyrolysis*, *155*, 105071.

**11.** Zhou, Y., Li, Z., Ji, L., Wang, Z., Cai, L., Guo, J., ... & Piotrowski, A. M. (2022). Facile preparation of alveolate biochar derived from seaweed biomass with potential removal performance for cationic dye. *Journal of Molecular Liquids*, *353*, 118623.

**12.** Li, Y., Gupta, R., Zhang, Q., & You, S. (2023). Review of biochar production via crop residue pyrolysis: Development and perspectives. *Bioresource technology*, *369*, 128423.

**13.** Tomczyk, A., Sokołowska, Z., & Boguta, P. (2020). Biochar physicochemical properties: pyrolysis temperature and feedstock kind effects. *Reviews in Environmental Science and Bio/Technology*, *19*(1), 191-215.

**14.** Li, X., Wang, T., Ma, Y., & Xu, R. (2023). Structural transformation of algal biochars during pyrolysis: Implications for contaminant adsorption. *Journal of Analytical and Applied Pyrolysis, 168*, 105799.

**15.** . He, D., Luo, Y., & Zhu, B. (2024). Feedstock and pyrolysis temperature influence biochar properties and its interactions with soil substances: Insights from a DFT calculation. *Science of the Total Environment*, *922*, 171259.

**16.** Farobie, O., Amrullah, A., Bayu, A., Syaftika, N., Anis, L. A., & Hartulistiyoso, E. (2022). In-depth study of bio-oil and biochar production from macroalgae Sargassum sp. via slow pyrolysis. *RSC advances*, *12*(16), 9567-9578.

**17.** Lou, B., Parker, M., & Roumeli, E. (2025). Effects of Pyrolysis Temperature of Macroalgal Biomass on the Structure and Mechanical Properties of Produced Biochar. *BioResources*, *20*(2).

**18.** Ippolito, J. A., Cui, L., Kammann, C., Wrage-Mönnig, N., Estavillo, J. M., Fuertes-Mendizabal, T., ... & Borchard, N. (2020). Feedstock choice, pyrolysis temperature and type influence biochar characteristics: a comprehensive meta-data analysis review. *Biochar*, *2*(4), 421-438.

**19.** Liu, Z., Dugan, B., Masiello, C. A., & Gonnermann, H. M. (2019). Biochar particle size, shape, and porosity act together to influence soil water properties. *PLOS ONE, 14*(3), e0214294.

**20.** Demirbas, A. (2004). Effects of temperature and particle size on bio-char yield from pyrolysis of agricultural residues. *Journal of analytical and applied pyrolysis*, *72*(2), 243-248.

**21.** Keiluweit, M., Nico, P. S., Johnson, M., & Kleber, M. (2010). Dynamic molecular structure of plant biomass-derived black carbon (biochar). *Environmental Science & Technology, 44*(4), 1247–1253.

**22.** Li, C., Zhang, C., Zhong, S., Duan, J., Li, M., & Shi, Y. (2023). The removal of pollutants from wastewater using magnetic biochar: a scientometric and visualization analysis. *Molecules*, *28*(15), 5840.

**23.** Mutić, S., Anojčić, J., Đukanović, N., Apostolović, T., Simetić, T., Petrović, J., & Beljin, J. (2025). *Exploring wood-derived biochar potential for electrochemical sensing of fungicides mancozeb and maneb in environmental water samples*. Talanta, 287, 127648.

**24.** Zhang, M., Gao, B., Yao, Y., Xue, Y., & Inyang, M. (2012). Synthesis of porous MgO-biochar nanocomposites for removal of phosphate and nitrate from aqueous solutions. *Chemical Engineering Journal*, *210*, 26-32.

**25.** Acharya, B. S., Dodla, S., Wang, J. J., Pavuluri, K., Darapuneni, M., Dattamudi, S., ... & Kharel, G. (2024). Biochar impacts on soil water dynamics: knowns, unknowns, and research directions. *Biochar*, *6*(1), 34

**26.** Weber, K., & Quicker, P. (2018). Properties of biochar. *Fuel*, *217*, 240-261.

**27.** Yuan, J. H., Xu, R. K., & Zhang, H. (2011). The forms of alkalis in the biochar produced from crop residues at different temperatures. *Bioresource technology*, *102*(3), 3488-3497.

**28.** Sudarsan, J. S., Goel, M., Jahangiri, H., Rout, P. R., Tavakolian, M., Briggs, C., ... & Nithiyanantham, S. (2025). Sustainable food waste management: a critical review on biochar production and applications. *Sustainable Food Technology*, 3, 1723–1743

**29.** Varkolu, M., Gundekari, S., Omvesh, Palla, V. C. S., Kumar, P., Bhattacharjee, S., & Vinodkumar, T. (2025). Recent advances in biochar production, characterization, and environmental applications. *Catalysts*, *15*(3), 243.

**30.** Mondal, A. K., Hinkley, C., Krishnan, L., Ravi, N., Akter, F., Ralph, P., & Kuzhiumparambil, U. (2024). Macroalgae-based biochar: Preparation and characterization of physicochemical properties for potential applications. *RSC Sustainability*, *2*(6), 1828-1836.

**31.** Murtaza, G., Ahmed, Z., Eldin, S. M., Ali, B., Bawazeer, S., Usman, M., ... & Tariq, A. (2023). Biochar-Soil-Plant interactions: A cross talk for sustainable agriculture under changing climate. *Frontiers in Environmental Science*, *11*, 1059449.

**32.** Di Domenico, G., Bianchini, L., Di Stefano, V., Venanzi, R., Lo Monaco, A., Colantoni, A., & Picchio, R. (2024). New Frontiers for Raw Wooden Residues, Biochar Production as a Resource for Environmental Challenges. *C*, *10*(2), 54.

**33.** Khater, E. S., Bahnasawy, A., Hamouda, R., Sabahy, A., Abbas, W., & Morsy, O. M. (2024). Biochar production under different pyrolysis temperatures with different types of agricultural wastes. *Scientific Reports*, *14*(1), 2625.

**34.** Buss, W., Wurzer, C., Manning, D. A., Rohling, E. J., Borevitz, J., & Mašek, O. (2022). Mineral-enriched biochar delivers enhanced nutrient recovery and carbon dioxide removal. *Communications Earth & Environment*, *3*(1), 67.

**35.** Zhang, J., Wang, B., Jin, J., Yang, S., & Li, G. (2022). A review of the microporous layer in proton exchange membrane fuel cells: Materials and structural designs based on water transport mechanism. *Renewable and Sustainable Energy Reviews*, *156*, 111998.

**36.** Arora, J., Joshi, A., & Ray, R. C. (2024). *Transforming agriculture residues for sustainable development*. Springer. https://doi. org/10.1007/978-3-031-61133-9.

**37.** Animali, L., Corrado, S., Mitillo, N., Tuccimei, P., Bartoli, M., Mattei, M., & Giorcelli, M. (2025). Characterization and evaluation of commercial biochar for surface water purification. *Sustainable Horizons*, *15*, 100145.

**38.** Petrović, J., Simić, M., Mihajlović, M., Koprivica, M., Kojić, M., & Nuić, I. (2021). Upgrading fuel potentials of waste biomass via hydrothermal carbonization. *Hemijska Industrija, 75*(5), 297–305

**39.** Li, L., Long, A., Fossum, B., & Kaiser, M. (2023). Effects of pyrolysis temperature and feedstock type on biochar characteristics pertinent to soil carbon and soil health: A meta-analysis. *Soil Use and Management*, *39*(1), 43-52.

**40.** Jung, K. W., Kim, K., Jeong, T. U., & Ahn, K. H. (2016). Influence of pyrolysis temperature on characteristics and phosphate adsorption capability of biochar derived from waste-marine macroalgae (Undaria pinnatifida roots). *Bioresource technology*, *200*, 1024-1028.

**41.** Li, L., Wang, J., Sun, W., Peng, X., & Qi, X. (2025). Production of Algae-Derived Biochar and Its Application in Pollutants Adsorption—A Mini Review. *Separations*, *12*(2), 32.

**42.** Lin, H., Huang, Y., Jin, Q., Ma, T., & Dong, Y. (2025). Effects of biomass components and pyrolysis temperature on the adsorption properties of biochar for heavy metals: A review. *Journal of Analytical and Applied Pyrolysis*, 107321.

**43.** Amalina, F., Abd Razak, A. S., Krishnan, S., Zularisam, A. W., & Nasrullah, M. (2022). A comprehensive assessment of the method for producing biochar, its characterization, stability, and potential applications in regenerative economic sustainability–a review. *Cleaner Materials*, *3*, 100045.

**44.** Rajput, V., Saini, I., Parmar, S., Pundir, V., Kumar, V., Kumar, V., ... & Rustagi, S. (2024). Biochar production methods and their transformative potential for environmental remediation. *Discover Applied Sciences*, *6*(8), 408.

**45.** Devrajani, S. K., Ahmed, Z., Qambrani, N. A., Kanwal, S., Sundaram, U. M., & Mubarak, N. M. (2024). Mechanism of arsenic removal using brown seaweed derived

impregnated with iron oxide biochar for batch and column studies. *Scientific Reports*, *14*(1), 18102.

**46.** Mondal, A. K., Hinkley, C., Krishnan, L., Ravi, N., Akter, F., Ralph, P., & Kuzhiumparambil, U. (2024). Macroalgae-based biochar: Preparation and characterization of physicochemical properties for potential applications. RSC Sustainability, 2(6), 1828-1836.

**47.** Knijnenburg, J. T., Kasemsiri, P., Kaewpradit, W., Tarinta, T., Jantapa, W., Jeejaila, T., ... & Jetsrisuparb, K. (2024). Co-pyrolysis of biomass with magnesium and phosphorus: Effect of magnesium content on phosphate release from biochar-based fertilizers. Biomass Conversion and Biorefinery, 14(14), 15351-15361.

**48.** Singh, B., & Raven, M. D. (2017). 21 X-ray diffraction analysis of biochar. Biochar: a guide to analytical methods, p 245.

**49.** Khalid, R., Jamil, A., Younas, K., Rasheed, S., Ghaffour, N., & Nawaz, M. S. (2025). Removal of pesticide Lambda–Cyhalothrin from aqueous medium by Parthenium hysterophorus biochar with non–linear adsorption modeling. *Desalination and Water Treatment*, 101480.

**50.** Gomes, H., Bento, E., Tavares, M. D., Santos, Y., da Costa, J. G., do Nascimento, R., ... & Teixeira, R. (2025). Removal of Azoxystrobin and Deltamethrin from Water Using Activated Biochar from Moringa oleifera L. Wood: Synthesis, Characterization, and Adsorption Study. *Molecules*, *30*(13), 2757.

**51.** Oba, O. A., & Pasaoglulari Aydinlik, N. (2022). Preparation of mesoporous activated carbon from novel African walnut shells (AWS) for deltamethrin removal: kinetics and equilibrium studies. *Applied Water Science*, *12*(7), 149.

**52.** AOAC International (2023) Official Methods of Analysis, 21st edn. AOAC International, Rockville, MD

**53.** Nakhjavan, B., Bland, J., & Khosravifard, M. (2021). Optimization of a multiresidue analysis of 65 pesticides in surface water using solid-phase extraction by LC-MS/MS. *Molecules*, *26*(21), 6627

**54.** Yu, X. Y., Ying, G. G., & Kookana, R. S. (2009). Reduced plant uptake of pesticides with biochar additions to soil. Chemosphere, 76(5), 665-671.

## Tables and Figures

**Table 1: Seaweed biochar pyrolysis temperature and corresponding yield and pH**

| Sl. No | Temperature | Yield (%) | pH |
|---|---|---|---|
| 1. | 350°C | 49.1 ± 0.46 | 10.635 ± 0.13 |
| 2. | 500°C | 42.8 ± 0.64 | 11.41 ± 0.17 |
| 3. | 650°C | 39.6 ± 0.58 | 11.395 ± 0.23 |

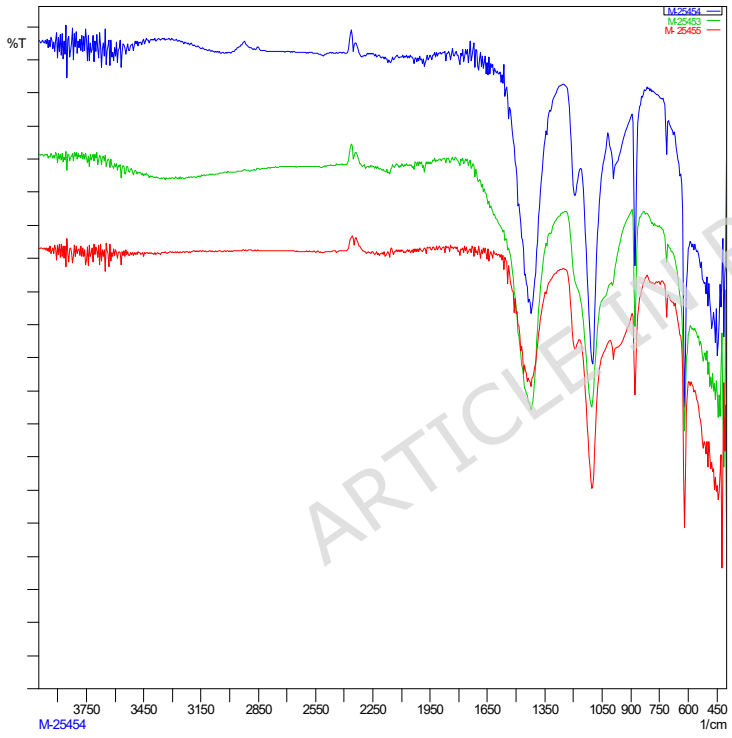




*Figure 1: FTIR spectra of biochar produced by pyrolysis at three different temperatures.*

**Table 2: Elemental composition of seaweed-derived biochar samples prepared at 350 °C pyrolysis temperatures, as determined by ICP-OES. Values are expressed as mean concentrations (ppm) with corresponding instrument standard deviations.**

| Elements | Units | Avg | Instrument Stddev |
|---|---|---|---|
| Al3961 | ppm | 4184.0 | 73.66 |
| As1937 | ppm | 48.03 | 0.6086 |
| B_2497 | ppm | 252.4 | 2.271 |
| Ba4554 | ppm | 34.98 | 0.3178 |
| Ca4226 | ppm | 28,464.0 | 253.6 |
| Cd2144 | ppm | 2.717 | 0.02513 |
| Co2286 | ppm | 3.259 | 0.04990 |
| Cr2835 | ppm | 12.96 | 0.2160 |
| Cu2247 | ppm | 7.958 | 0.1051 |
| Fe2599 | ppm | 2394.0 | 34.32 |
| K_7664 | ppm | 47,953.0 | 1601.0 |
| Li6707 | ppm | 3.087 | 0.09847 |
| Mg2852 | ppm | 13,428.0 | 177.1 |
| Mn2576 | ppm | 155.7 | 3.700 |
| Mo2020 | ppm | 0.4448 | 0.04283 |
| Na8183 | ppm | 39,850.0 | 107.8 |
| Ni2316 | ppm | 4.957 | 0.06770 |
| P_2136 | ppm | 1413.0 | 14.21 |
| Pb2203 | ppm | 2.505 | 0.1173 |
| Sr4077 | ppm | 1687.0 | 58.28 |
| Ti3349 | ppm | 50.66 | 1.801 |
| Zn2138 | ppm | 18.10 | 0.1399 |

**Table 3 : Elemental composition of seaweed-derived biochar samples prepared at 500 °C pyrolysis temperatures, as determined by ICP-OES. Values are expressed as mean concentrations (ppm) with corresponding instrument standard deviations.**

| Elem | Units | Avg | Instrument Stddev |
|---|---|---|---|
| Al3961 | ppm | 4895 | 25.71 |
| As1937 | ppm | 53.56 | 0.3048 |
| B_2497 | ppm | 284.9 | 2.070 |
| Ba4554 | ppm | 40.74 | 0.4708 |
| Ca4226 | ppm | 26072 | 1331 |
| Cd2144 | ppm | 1.203 | 0.01408 |
| Co2286 | ppm | 3.725 | 0.03727 |
| Cr2835 | ppm | 13.97 | 0.5120 |
| Cu2247 | ppm | 8.784 | 0.03438 |
| Fe2599 | ppm | 3019 | 52.17 |
| K_7664 | ppm | 45309 | 1615 |
| Li6707 | ppm | 2.623 | 0.06048 |
| Mg2852 | ppm | 13428 | 53.03 |
| Mn2576 | ppm | 193.4 | 3.338 |
| Mo2020 | ppm | 0.5730 | 0.009135 |
| Na8183 | ppm | 41456 | 179.7 |
| Ni2316 | ppm | 5.583 | 0.004767 |
| P_2136 | ppm | 1627 | 8.310 |
| Pb2203 | ppm | 2.028 | 0.1563 |
| Sr4077 | ppm | 1873 | 55.13 |
| Ti3349 | ppm | 115.3 | 1.704 |
| Zn2138 | ppm | 21.66 | 0.1069 |

**Table 4 : Elemental composition of seaweed-derived biochar samples prepared at 600 °C pyrolysis temperatures, as determined by ICP-OES. Values are expressed as mean concentrations (ppm) with corresponding instrument standard deviations.**

| Elem | Units | Avg (Mean) | Instrument Stddev |
|---|---|---|---|
| Al3961 | ppm | 4401 | 111.1 |
| As1937 | ppm | 70.62 | 0.6062 |
| B_2497 | ppm | 350.8 | 2.891 |
| Ba4554 | ppm | 52.43 | 0.3724 |
| Ca4226 | ppm | 27414 | 696.0 |
| Cd2144 | ppm | 0.5949 | 0.02007 |
| Co2286 | ppm | 4.189 | 0.03557 |
| Cr2835 | ppm | 13.66 | 0.4987 |
| Cu2247 | ppm | 9.857 | 0.1365 |
| Fe2599 | ppm | 2964 | 65.81 |
| K_7664 | ppm | 60112 | 2711 |
| Li6707 | ppm | 2.749 | 0.1542 |
| Mg2852 | ppm | 16749 | 77.57 |
| Mn2576 | ppm | 204.7 | 4.756 |
| Mo2020 | ppm | 0.7894 | 0.04932 |
| Na8183 | ppm | 52230 | 785.0 |
| Ni2316 | ppm | 5.985 | 0.09366 |
| P_2136 | ppm | 1953 | 18.41 |
| Pb2203 | ppm | 2.536 | 0.2417 |
| Sr4077 | ppm | 2558 | 37.22 |
| Ti3349 | ppm | 140.7 | 2.718 |
| Zn2138 | ppm | 22.19 | 0.3657 |

**Table 5: Zeta-potential value obtained for biochar samples**

| Biochar Sample | Pyrolysis Temperature | pH | Zeta Potential |
|---|---|---|---|
| Biochar Sample A | 350 °C | 7 | -3.03mV |
| Biochar Sample B | 500 °C | 7 | -1.28 mV |
| Biochar Sample C | 600 °C | 7 | -7.93mV |

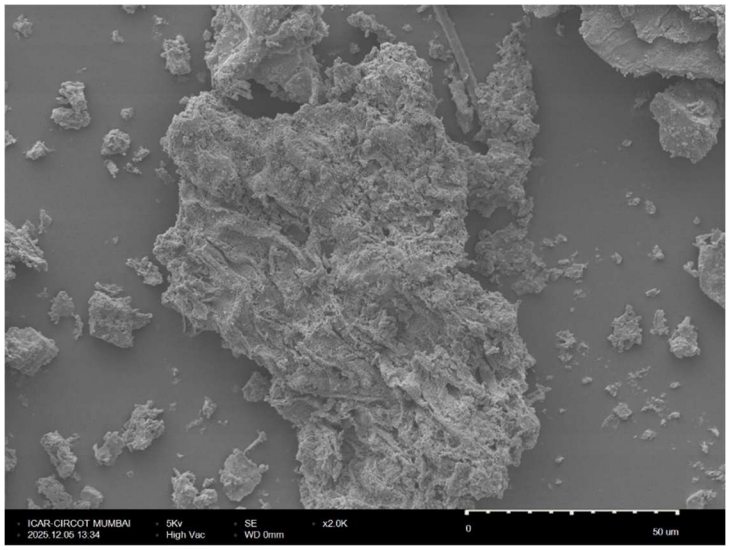


*Figure 2: SEM Image of Seaweed Biochar under pyrolysis at 350 ℃*

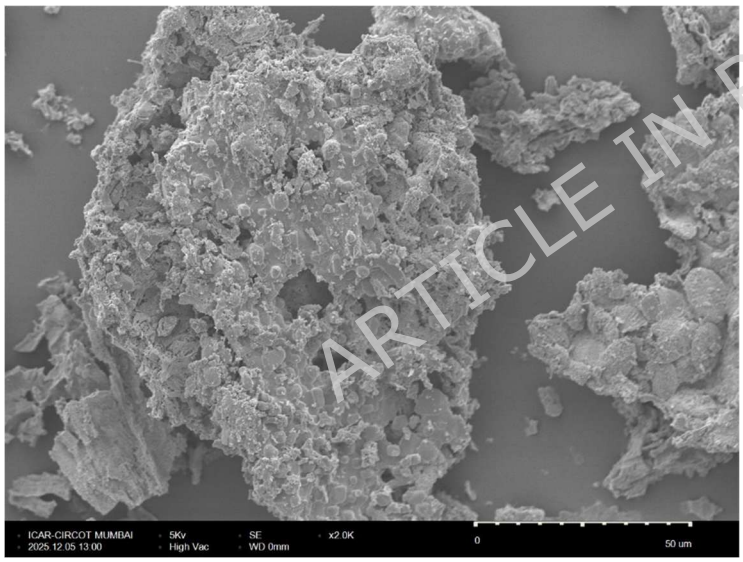


*Figure 3: SEM Image of Seaweed Biochar developed under pyrolysis at 500℃*

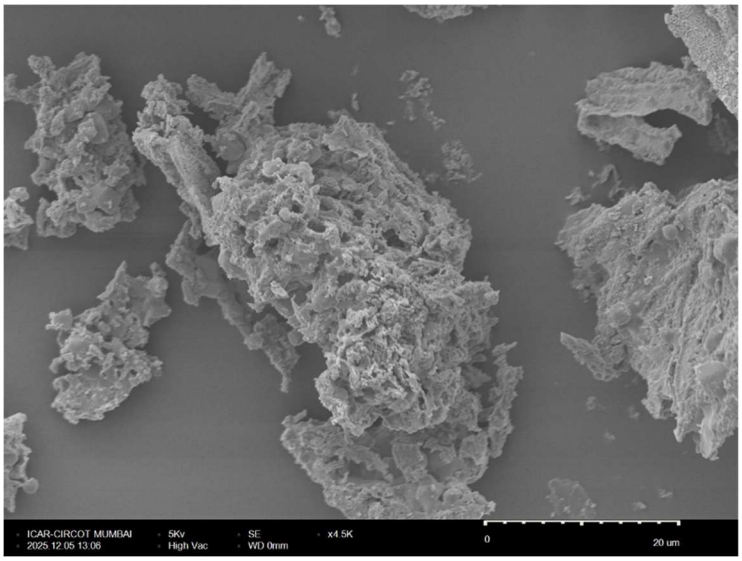


*Figure 4: SEM Image of Seaweed biochar developed under pyrolysis at 600 ℃*

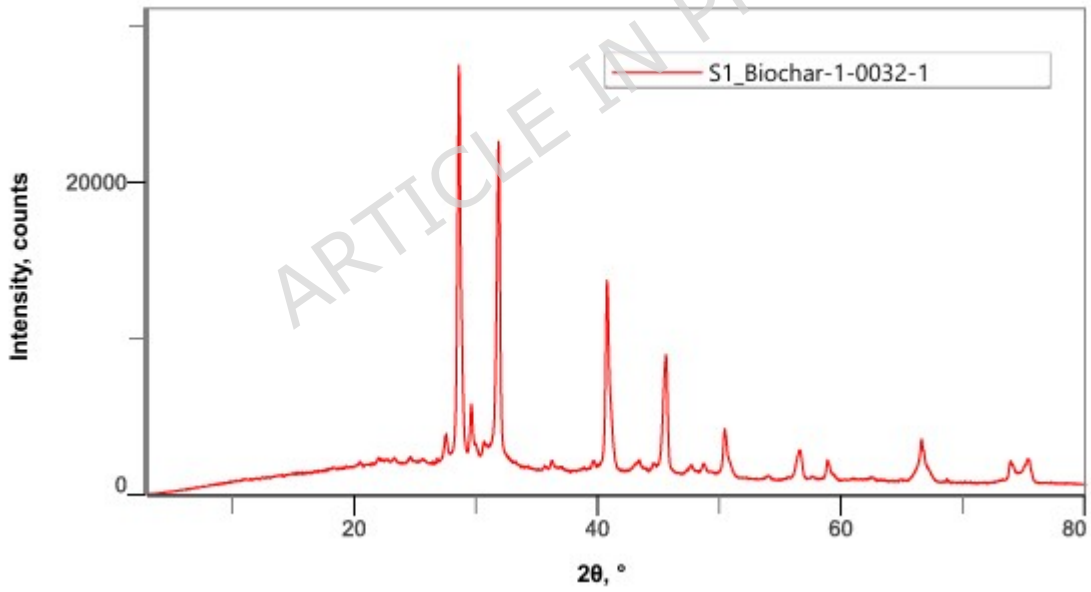


*Figure 5: XRD characterization of seaweed biochar developed under pyrolysis at 350℃*

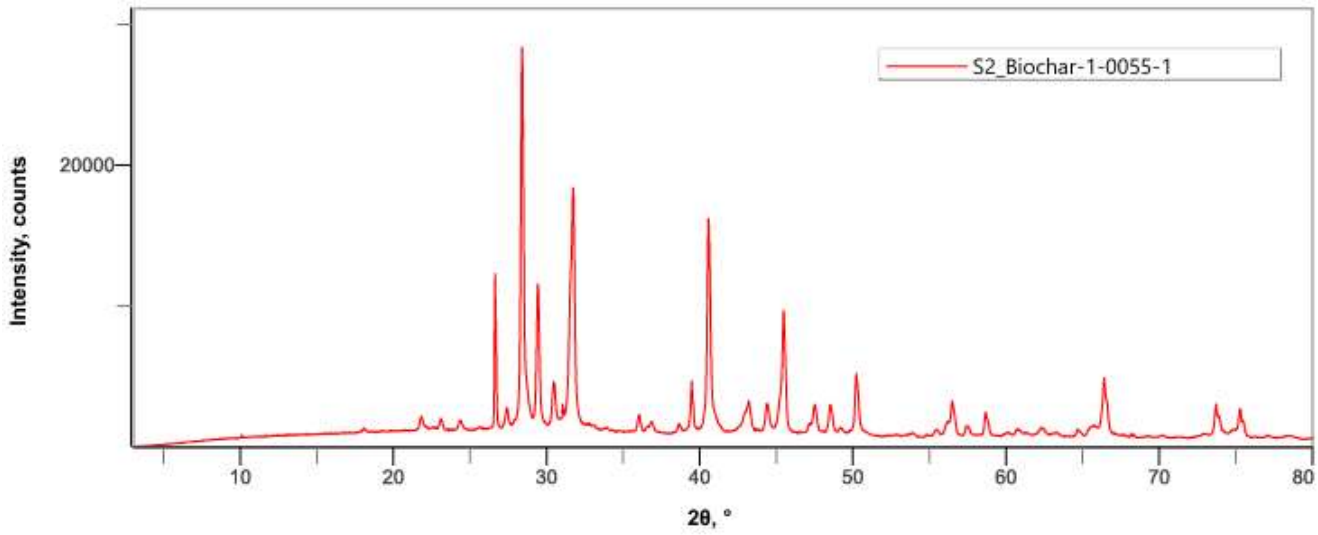


*Figure 6: XRD characterization of seaweed biochar developed under pyrolysis at 500℃*

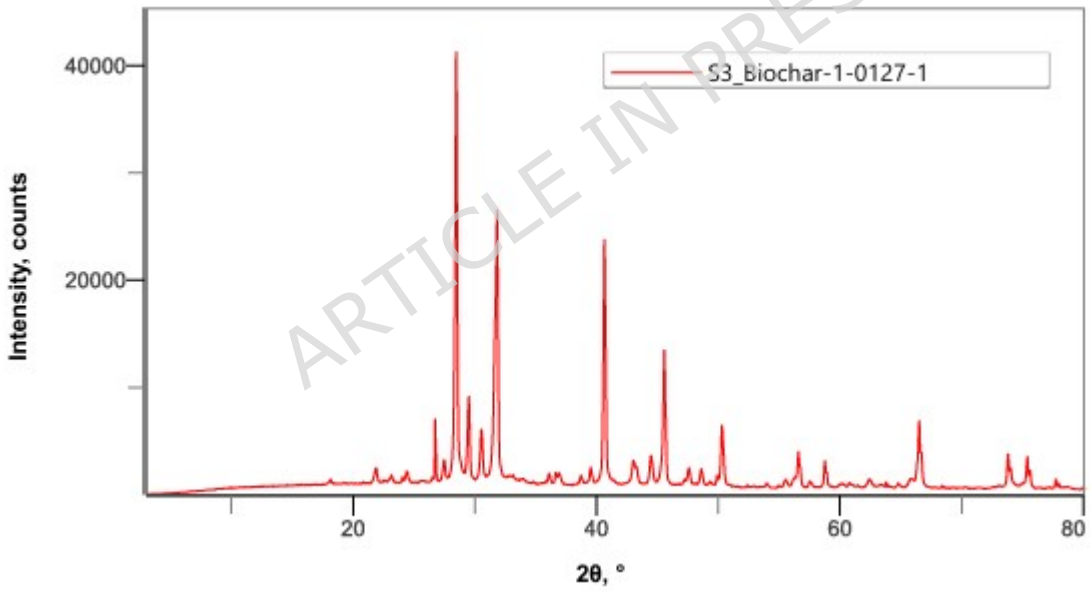




*Figure 7: XRD characterization of seaweed biochar developed under pyrolysis at 600 ℃*

**Table 6. Concentration of cypermethrin and deltamethrin in spiked water treated with seaweed biochar prepared at different pyrolysis temperatures**

| Pyrolysis Temperature (°C) | Sampling Day | Cypermethrin (µg/L) | Deltamethrin (µg/L) |
|---|---|---|---|
| **350 °C** | 0th day | 650.25 | 771.60 |
| | 6th day | 0.21 | 0.19 |
| **500 °C** | 0th day | 675.77 | 820.26 |
| | 6th day | 0.081 | 0.065 |
| **600 °C** | 0th day | 463.72 | 731.09 |
| | 6th day | 0.088 | 0.050 |